# *NMR Solution Structure and Condition-Dependent Oligomerization of the Antimicrobial Peptide Human Defensin 5*

Published in final edited form as:
*Biochemistry*. 2012 December 4; 51(48): 9624–9637. doi:10.1021/bi301255u.

# NMR Solution Structure and Condition-Dependent Oligomerization of the Antimicrobial Peptide Human Defensin 5

**Andrew J. Wommack**[1], **Scott A. Robson**[2], **Yoshitha A. Wanniarachchi**[1], **Andrea Wan**[1], **Christopher J. Turner**[3], **Gerhard Wagner**[2], and **Elizabeth M. Nolan**[1,*]

[1]Department of Chemistry, Massachusetts Institute of Technology, Cambridge, MA 02139

[2]Department of Biological Chemistry and Molecular Pharmacology, Harvard Medical School, 240 Longwood Avenue, Boston, Massachusetts 02115

[3]Francis Bitter Magnet Laboratory, Massachusetts Institute of Technology, Cambridge, MA 02139

## Abstract

Human defensin 5 (HD5) is a 32-residue host-defense peptide expressed in the gastrointestinal, reproductive, and urinary tracts that has antimicrobial activity. It exhibits six cysteine residues that are regiospecifically oxidized to form three disulfide bonds ($Cys^3$—$Cys^{31}$, $Cys^5$—$Cys^{20}$, and $Cys^{10}$—$Cys^{30}$) in the oxidized form ($HD5_{ox}$). To probe the solution structure and oligomerization properties of $HD5_{ox}$, and select mutant peptides lacking one or more disulfide bonds, NMR solution studies and analytical ultracentrifugation experiments are reported in addition to *in vitro* peptide stability assays. The NMR solution structure of $HD5_{ox}$, solved at pH 4 in 90:10 $H_2O/D_2O$, is presented (PDB: 2LXZ). Relaxation $T_1/T_2$ measurements and the rotational correlation time ($\tau_c$) estimated from a [$^{15}$N,$^1$H]-TRACT experiment demonstrate that $HD5_{ox}$ is dimeric under these experimental conditions. Exchange broadening of the Hα signals in the NMR spectra suggests that residues 19-21 ($Val^{19}$-$Cys^{20}$-$Glu^{21}$) contribute to the dimer interface in solution. Exchange broadening is also observed for residues 7-14 comprising the loop. Sedimentation velocity and equilibrium studies conducted in buffered aqueous solution reveal that the oligomerization state of $HD5_{ox}$ is pH-dependent. Sedimentation coefficients of ca. 1.8 S and a molecular weight of 14,363 Da were determined for $HD5_{ox}$ at pH 7, supporting a tetrameric form ($[HD5_{ox}] \geq 30$ μM). At pH 2, a sedimentation coefficient of ca. 1.0 S and a molecular weight of 7,079 Da, corresponding to a $HD5_{ox}$ dimer, were obtained. Millimolar concentrations of NaCl, $CaCl_2$, and $MgCl_2$ have negligible effect on the $HD5_{ox}$ sedimentation coefficients in buffered aqueous solution at neutral pH. Removal of a single disulfide bond results in a loss of peptide fold and quaternary structure. These biophysical investigations highlight the dynamic and environment-sensitive behavior of $HD5_{ox}$ in solution, and provide important insights into $HD5_{ox}$ structure/activity relationships and the requirements for antimicrobial action.

Host-defense peptides and proteins are key players in the mammalian innate immune response, and serve to prevent colonization by invading pathogenic microbes.[1-5] Human defensins are ribosomally-synthesized, cysteine-rich, host-defense peptides expressed in neutrophils (human neutrophil peptides, HNPs) and various types of epithelial cells (α- and β-defensins).[6-9] Human defensin 5 (HD5), the focus of this work, is an α-defensin comprised of thirty-two amino acids that exhibits three regiospecific disulfide bonds with the connectivities $Cys^3$—$Cys^{31}$, $Cys^5$—$Cys^{20}$, and $Cys^{10}$—$Cys^{30}$ in the oxidized form,

*Corresponding author: lnolan@mit.edu, Phone: 617-452-2495, Fax: 617-324-0505.

**SUPPORTING INFORMATION AVAILABLE**

Tables S1-S9 and Figures S1-S47. This information is available free of charge via the Internet at http://pubs.acs.org.

hereafter $HD5_{ox}$ (Figure 1). Like other α-defensins, the $HD5_{ox}$ disulfide array confers a three-stranded β-sheet structure[10] and protease resistance.[11,12]

HD5 is expressed in the human gastrointestinal,[13-16] reproductive,[17] and urinary[18] tracts. Small intestinal Paneth cells,[19] which reside at the base of the crypts of Lieberkühn throughout the small intestine and serve to protect the intestinal epithelium and stem cells from invading microbes, package the HD5 propeptide in subcellular granules.[15,20] The 75-aa propeptide is converted into the 32-aa mature form by trypsin-catalyzed proteolysis of the N-terminal 43-aa pro region, and HD5 is released into the intestinal lumen in response to microbial invasion.[21] Numerous *in vitro* studies demonstrated that $HD5_{ox}$ exhibits antimicrobial activity against a variety of Gram-negative and -positive human pathogens including *Escherichia coli*, *Salmonella enterica*, *Bacillus cereus*, *Listeria monocytogenes*, *Staphylococcus aureus*, and *Enterococcus facieum.*[10,22,23] A HD5 transgenic mouse, which expresses HD5 only in the small intestinal Paneth cells, survived oral *Salmonella* challenge ($1.5 \times 10^9$ cfu/mL) at levels that were lethal for the wild-type mouse.[24] This observation supports an antibacterial role for HD5 *in vivo*. Recent HD5 transgenic mouse studies of the commensal microbiota revealed that HD5 expression modulates the composition of the resident microflora.[25] Defensin deficiency has been observed in patients with inflammatory diseases of the small bowel.[26] A single R13H point mutation in HD5 was observed in a Crohn's disease patient, and this mutation afforded attenuated cell killing for some bacterial species *in vitro*.[27] Indeed, an *E. coli* Nissle 1917 strain engineered to biosynthesize and secrete HD5 was recently reported as a possible probiotic therapy for Crohn's disease and other inflammatory diseases of the bowel.[28,29] Antiviral activities of $HD5_{ox}$ are also documented.[30-32] For instance, $HD5_{ox}$ blocks infection by various non-enveloped human viruses including adenoviruses[31,32] and sexually transmitted papillomaviruses,[30] and may provide a natural barrier to certain viral diseases in the female reproductive system.

The broad-range antibacterial and -viral activities of $HD5_{ox}$, in addition to other putative physiological roles, motivate investigations of structure-activity relationships. To date, these studies have addressed the importance of the arginine residues,[27] the role of the canonical salt bridge formed by $Arg^6$—$Glu^{14}$,[11] and the disulfide array.[12,33] The antibacterial activity of the D-enantiomer, prepared by solid-phase peptide synthesis, was also evaluated and exhibited species-specific activity.[34] A recent alanine scan identified $Leu^{29}$ as a critical determinant for antibacterial activity.[35] Taken together, these investigations overwhelmingly support a model whereby the mechanism of $HD5_{ox}$ action differs for Gram-negative (e.g. *E. coli*) and -positive (e.g. *S. aureus*) organisms. Whereas a variety of HD5 mutant peptides, including the D-enantiomer and disulfide deletion mutants, retain activity against *E. coli*, the ability of these peptides to kill *S. aureus* is severely attenuated.[12,33,34] $HD5_{ox}$ disrupts the Gram-negative inner membrane;[12] however, the precise details of its mechanism of action against *E. coli* and other Gram-negative organisms, in addition to how it acts on Gram-positive species, are unclear. Extensive mutagenesis studies of the human neutrophil α-defensin HNP1[36-40] and the murine Paneth cell α-defensin cryptdin-4 (Crp4)[41-46] have been presented. In total, these studies delineate that defensin structure/activity relationships must be considered on a case-by-case basis, and highlight the importance of evaluating both electrostatics and hydrophobicity when considering the antimicrobial and -viral activities of human α-defensin peptides.[4]

We previously reported a $HD5_{ox}$ mutant peptide family where pairs of Cys residues involved in native disulfide linkages were systematically mutated to Ser/Ala residues.[12] Many of these mutants retained antibacterial activity against *E. coli* ATCC 25922 whereas none provided activity against *S. aureus* ATCC 25923 over the concentration range tested. In addition, removal of one or more disulfide bonds markedly attenuated protease resistance. We therefore hypothesized that the lack of antibacterial activity observed for the mutant

peptides against *S. aureus* may result from (i) mutant peptide instability under the assay conditions, (ii) disruption of quaternary structure, an/or (iii) failure to interact with a specific and as-yet unidentified cellular target.

Herein we address these possibilities and report extensive biophysical studies designed to probe the solution structure and dynamics of $HD5_{ox}$ and select disulfide mutant peptides (Figure 1). We present the NMR solution structure of native $HD5_{ox}$ in addition to NMR studies of $^{15}N$-$HD5[Ser^{3,31}]_{ox}$, $^{15}N$-$HD5[Ser^{10,30}]_{ox}$, and $^{15}N$-$HD5_{red}$. We also describe the quaternary structure of $HD5_{ox}$ and disulfide mutants by using a combination of NMR dynamics measurements, rotation correlation time measurements, and analytical ultracentrifugation. These investigations demonstrate that the native disulfide array is essential for $HD5_{ox}$ quaternary structure, and that the $HD5_{ox}$ oligomerization state in aqueous solution is condition-dependent.

## EXPERIMENTAL PROCEDURES

### Materials and General Methods

All solvents, reagents, and chemicals were purchased from commercial suppliers and used as received unless noted otherwise. Deuterated water ($D_2O$), $^{15}N$-ammonium chloride, and U-$^{13}C$-glucose were purchased from Cambridge Isotopes (Cambridge, MA). All aqueous solutions, buffers, and NMR samples were prepared with Milli-Q water (18.2 $m\Omega cm^{-1}$) that was passed through a 0.22 μm filter before use. Unlabeled HD5 and mutant peptides were overexpressed as $His_6$-fusion proteins in *E. coli* BL21(DE3) and were purified as previously described.[12]

### General Instrumentation

Analytical and semi-preparative high-performance liquid chromatography (HPLC) were performed on an Agilent 1200 instrument equipped with a thermostated autosampler set at 4 °C and thermostated column compartment generally set at 20 °C, and a multi-wavelength detector set at 220 and 280 nm (500 nm reference wavelength unless noted otherwise). Preparative HPLC was performed using an Agilent PrepStar 218 instrument outfitted with an Agilent ProStar 325 UV-Vis dual-wavelength detector set at 220 and 280 nm. A Clipeus C18 column (5 μm pore, 4.6 × 250 mm, Higgins Analytical, Inc.) set at a flow rate of 1 mL/min was employed for all analytical HPLC experiments. A ZORBAX C18 column (5 μm pore, 4.6 × 250 mm, Agilent Technologies, Inc.) set at a flow rate of 5 mL/min was employed for all semi-preparative-scale HPLC purification. A Luna 100 Å C18 LC column (10 μm pore, 21.2 × 250 mm, Phenomenex) operated at 10 mL/min was utilized for all preparative-scale HPLC purification. HPLC-grade acetonitrile (MeCN) and HPLC-grade trifluoroacetic acid (TFA) were routinely purchased from EMD. For all HPLC separations, solvent A was 0.1% TFA/$H_2O$ and solvent B was 0.1% TFA/MeCN. These solvents were passed through a 0.2-μm filter prior to use. High-resolution mass spectrometry was performed by using an Agilent LC/MS system comprised of an Agilent 1260 series LC system outfitted with an Agilent Poroshell 120 EC-C18 column (2.7 μm pore size) and an Agilent 6230 TOF system housing an Agilent Jetstream ESI source. LC/MS-grade MeCN containing 0.1% formic acid and LC/MS-grade water containing 0.1% formic acid were obtained from J. T. Baker. For all LC/MS analyses, solvent A was 0.1% formic acid/$H_2O$ and solvent B was 0.1% formic acid/MeCN. The samples were analyzed by using a gradient of 5-95% B over five min with a flow rate of 0.4 mL/min. The MS profiles were analyzed and deconvoluted by using Agilent Technologies Quantitative Analysis 2009 software version B.03.02. A BioTek Synergy HT plate reader outfitted with a calibrated BioTek Take3 Multi-Volume Plate was employed for optical absorption measurements. Peptide stock solution concentrations were routinely quantified by using the calculated extinction

coefficients for $HD5_{ox}$ or mutant peptide (Table S1, Supporting Information). Solution and buffer pH values were verified by using either a Mettler Toledo S20 SevenEasy pH meter or a HANNA Instruments HI 9124 pH meter equipped with a microelectrode.

## Overexpression and Purification of $^{15}N$ and $^{13}C,^{15}N$-Labeled Peptides

The plasmids employed for the overexpression of $His_6$-Met-HD5, $His_6$-Met-HD5[$Ser^{3,31}$], and $His_6$-Met-HD5[$Ser^{10,30}$] are based on the pET-28b expression vector and are described elsewhere.[12] Each expression plasmid was transformed into homemade chemically-competent *E. coli* BL21(DE3) cells and freezer stocks were prepared from single colonies. For large-scale overexpression of $^{15}N$-labeled peptides, a 50-mL overnight culture was prepared by inoculating LB media containing 50 μg/mL kanamycin from a freezer-stock of the desired *E. coli* overexpression strain. The starter culture was grown for 16 h (37 °C, 175 rpm) and the $OD_{600}$ recorded to confirm that the cultures reached saturation ($OD_{600}$ ~ 1.5). Aliquots (20 mL) of the overnight culture were centrifuged (3,600 rpm × 10 min, 4 °C) and the supernatant was discarded. The resulting cell pellets were resuspended in 3 mL of sterile-filtered $^{15}N$-labeled M9 minimal medium (6.0 g/L disodium phosphate, 3.0 g/L monopotassium phosphate, 0.5 g/L sodium chloride, 1.0 g/L $^{15}N$-labeled ammonium chloride) supplemented with 2 mL/L of 1 M $MgSO_4$, 2 mL/L of 5 mM $FeCl_3$, 100 μL/L of 1M $CaCl_2$, 1 mL/L of glycerol, 2.0 g/L of D-glucose, 1 mL/L of 50 mg/mL kanamycin, and 200 μL of a vitamin mix.[47] The vitamin mix contained choline chloride (200 mg), folic acid (250 mg), pantothenic acid (250 mg), nicotinamide (250 mg), myo-inositol (50 mg), pyridoxal hydrochloride (250 mg), thiamin hydrochloride (250 mg), riboflavin (25 mg), adenosine (50 mg), and biotin (50 mg) suspended in 7.5 mL of sterile-filtered Milli-Q water. The resuspended bacterial cell pellet was used to inoculate 1 L of the same minimal medium and the resulting cultures were grown at 37 °C with shaking at 175 rpm in 4 L baffled flasks. Protein expression was induced by addition of IPTG (0.5 mL of a 0.5 M aqueous stock solution, 250 μM final concentration) at $OD_{600}$ ~ 0.6 (t ~ 5.5 h). The cultures were incubated at 37 °C with shaking at 175 rpm for an additional 4 h, and the cells were immediately pelleted by centrifugation (4,000 rpm × 30 min, 4 °C). $^{15}N$-labeled $HD5_{ox}$ was overexpressed on a 4-L scale and the $^{15}N$-labeled mutant peptides were each overexpressed on a 12-L scale. The final $OD_{600}$ values varied from ca. 0.7 to ca. 1.2 depending on the shaker flask. The resulting cell pellets were collected, flash frozen in liquid $N_2$, and stored at -80 °C. The wet pellet yield for $^{15}N$-$His_6$-Met-HD5 was ca. 2 g/L culture. Wet pellet yields of ca. 1.2 and ca.1.8 g/L culture were obtained for 15N-$His_6$-Met-HD5[$Ser^{3,31}$] and $^{15}N$-$His_6$-HD5[$Ser^{10,30}$], respectively. Overexpression of double-labeled $^{13}C,^{15}N$-$His_6$-Met-HD5 was performed on a 6-L scale by using the same method and substituting U-$^{13}C$-glucose for unlabeled glucose.

Isotopically-labeled $His_6$-HD5 and the His-tagged mutant peptides were purified as described previously for the unlabeled congeners.[12] In brief, the $His_6$-tagged HD5 and serine double mutants were isolated in yields of ca. 5-15 mg/L culture following Ni-NTA affinity chromatography. Each $His_6$ tag was cleaved by using cyanogen bromide, and each crude peptide reduced by addition of TCEP and HPLC purified. An oxidative folding procedure was employed to obtain the oxidized forms, which were separated and purified by semi-preparative HPLC.[12] Peptide purity was ascertained by analytical HPLC (Figures S1-S4), and peptide identities were confirmed by mass spectrometry (Table S2). The purified peptides were lyophilized to dryness and stored as powders at −20 °C until use. Some disulfide bond shuffling was observed by analytical HPLC for select unlabeled disulfide deletion mutants after several months of storage at -20 °C in neutral aqueous solution. As a result, the $^{15}N$-labeled disulfide regioisomers of the serine double mutants were stored as lyophilized powders until use, and characterized immediately following purification.

### Peptide Stability in the Presence of *Staphylococcus aureus*

*S. aureus* ATCC 25923 was grown overnight with shaking (37 °C, 16 h) in 5 mL of TSB. The overnight culture was diluted 1:100 into 6 mL of fresh TSB and grown for ~2 h at 37 °C with shaking at 150 rpm until the $OD_{650}$ reached ~0.6. A 5-mL portion of the culture was transferred to a sterile culture tube and centrifuged (3500 rpm × 10 min, 4 °C) to pellet the bacterial cells. The supernatant was discarded and the cell pellet was resuspended in 5 mL of AMA buffer (10 mM sodium phosphate buffer supplemented with 1% TSB, pH 7.4). The cell suspension was centrifuged (3500 rpm × 10 min, 4 °C) and the supernatant discarded. The resulting cell pellet was resuspended in 5 mL of AMA buffer and diluted with AMA buffer to obtain an $OD_{650}$ value of 0.6 ($1 \times 10^8$ CFU/mL). This bacterial suspension was further diluted 1:100 in two steps (1:10 × 1:10) into 2 mL of AMA buffer. The diluted cultures were used immediately.

Peptide stability assays were performed in 96-well plates. Each well contained 10 μL of a 200-μM (10x) aqueous sterile-filtered peptide stock solution or a no-peptide control. A 90-μL aliquot of the diluted bacterial culture was added to each well and the plate was incubated for 1 h (37 °C, 150 rpm). Wells containing AMA buffer only and peptide in the AMA buffer without *S. aureus* were also included. Immediately after the 1 h incubation, each culture was transferred to a microcentrifuge tube and the samples were centrifuged (13,000 rpm × 10 min, 4 °C). The supernatants were transferred to new microcentrifuge tubes, a 10-μL aliquot of 2% aqueous TFA was added to each solution, and the samples were centrifuged (13,000 rpm × 10 min, 4 °C). The resulting supernatants were transferred to HPLC vials and stored in an autosampler thermostated at 4 °C until analytical HPLC analysis (10-60% B over 30 min). This assay was conducted at least in triplicate for each peptide and over two separate days. Representative HPLC traces are reported in Figures 2 and S5-S6.

### Solution NMR Sample Preparation

Samples of $^{15}$N-HD5$_{ox}$ were prepared at different concentrations and pH values to determine the optimal sample conditions for NMR data collection. Initial data acquisition was performed on a 460-μM sample of $^{15}$N-HD5$_{ox}$ that was dissolved in 90:10 $H_2O/D_2O$ immediately after HPLC purification and lyophilization (Figure 3). Additional samples of $^{15}$N-HD5$_{ox}$ were prepared at pH 5.0 (630, 460, and 260 μM) by using an aqueous solution of 1 N HCl for adjusting the sample pH. In a separate screen, $^{15}$N-HD5$_{ox}$ samples at pH 7.0 (333 μM), 6.0 (340 μM), 5.0 (400 μM), and 4.0 (460 μM) in 90:10 $H_2O/D_2O$ were prepared by using TFA to adjust pH as necessary. To determine the effect of buffer, samples of $^{15}$N-HD5$_{ox}$ (800 μM) were prepared in 20 mM Tris-HCl buffer containing 10% $D_2O$ (v/v) at pH = 7.0, 6.0, and 5.0. Lastly, $^{15}$N-HD5$_{ox}$ (880 μM) was prepared in 10 mM sodium phosphate buffer with 10% $D_2O$ (v/v) at pH = 7.0, 6.0, and 4.0. In these two sets of samples, the sample pH was adjusted by incremental additions of 1N HCl. Based on the $^1$H,$^{15}$N-HSQC spectra of $^{15}$N-HD5$_{ox}$ prepared under various conditions, the $^{13}$C,$^{15}$N-HD5$_{ox}$ sample (340 μM) was prepared in 90:10 $H_2O/D_2O$ at pH 4, and TFA was employed to adjust the sample pH. These conditions afforded the greatest peak dispersion, and twenty-eight of thirty-one amide resonances were observed for $^{13}$C,$^{15}$N-HD5$_{ox}$ in the $^1$H,$^{15}$N-HSQC. Likewise, all $^{15}$N-HD5[Ser$^{3,31}$]$_{ox}$ and $^{15}$N-HD5[Ser$^{10,30}$]$_{ox}$ regioisomers were prepared in 90:10 $H_2O/D_2O$ at pH 4. The NMR sample of $^{15}$N-HD5$_{red}$ (650 μM) was prepared in 90:10 $H_2O/D_2O$ containing 20 μM TFA to ensure that the peptide remained reduced.

### Solution NMR Spectroscopic Studies

All 1-D $^1$H NMR spectra were collected on a Varian 500 MHz spectrometer housed in the MIT Department of Chemistry Instrumentation Facility (DCIF) that was operated at an

ambient probe temperature of 293 K (Figures S7-S8). Standard techniques for water suppression and data acquisition were employed. A number of multi-dimensional NMR spectra were recorded on a 600 MHz NMR spectrometer housed in the MIT Francis Bitter Magnet Laboratory (FMBL) based on a FBML narrow bore magnet and a console designed and constructed by members of the FBML. This spectrometer is equipped with three transmitter channels, and a Nalorac 5 mm indirect triple resonance $^{1}H[^{13}C,^{15}N]$ probe with z-gradient. Additional multi-dimensional NMR spectra were recorded on a 600 MHz Bruker Avance spectrometer equipped with a cryogenic probe housed at Harvard Medical School. To determine optimal acquisition conditions for $HD5_{ox}$ , $^{1}H,^{15}$ N-HSQC experiments were performed at 15 °C, 20 °C, and 25 °C. For the initial resonance assignments, TOCSY and NOESY experiments were performed at 25 °C. 2-D TOCSY spectra were recorded with mixing times of 30 and 60 ms, and 2-D NOESY spectra were recorded with mixing times of 150, 200, and 400 ms. All experiments were acquired with 2048 complex points in $t_2$ and 512 complex points in $t_1$, and a sweep width of 12 ppm in both dimensions. The 3-D $^{15}$N-edited TOCSY and 3-D $^{15}$N-edited NOESY experiments were collected with 60 ms and 200 ms mixing times, respectively. A 200 ms mixing time was also employed for a 3-D $^{13}$C-edited NOESY experiment. Sequence-specific assignment was aided by the collection of standard HNCA, HNCO, and HNCACO pulse sequences; however, non-uniform sampling was used. Specifically, a matrix of 38 points ($^{15}$N dimension) by 40 points ($^{13}$C dimension) at the ca. 20% levels (a total of 320 acquired complex points) was sub-sampled. The sampling schedule was created based on the Poisson Gap sampling method.[48] Missing data points were reconstructed by using the istHMS algorithm.[49] Only 1-D $^{1}$H NMR and 2-D $^{1}H,^{15}$N-HSQC spectra for the $HD5[Ser^{3,31}]_{ox}$ and $HD5[Ser^{10,30}]_{ox}$ regioisomers were collected, and the HSQC experiments were conducted over a temperature range of 15 to 25 °C. Spectral data were processed by using NMRPipe[50] and analyzed by using Sparky[51] or CARA.[52]

## NMR Solution Structure Calculations and Refinement

Structure calculations were initially performed in CYANA to fully assign NOE crosspeaks and establish the hydrogen bond network by inference from preliminary structures along with NOE patterns. These NOE assignments were then used in structure calculations with X-PLOR NIH using explicit water refinement. During this calculation, the system was cooled from 3000 to 25 K within 10 psec, applying the high force constants obtained at the end of the previous cooling stage. The experimental restraints included 421 upper distance limits, fifty-four dihedral angles identified by analysis of backbone chemical shifts by the program TALOS,[53] sixteen $X_1$ angles, three disulfide bonds, and fifteen hydrogen bonds.

Of the 400 structures resulting from the final round of structure calculation, the twenty lowest-energy structures were selected. The geometry and elements of secondary structure were analyzed using PROCHECK.[54] These coordinates are deposited in the Protein Data Bank (code: 2LXZ). The UCSF Chimera[55] package and MOLMOL[56] were employed for final graphical presentation.

## Sedimentation Velocity Experiments

A Beckman XL-I Analytical Ultracentrifuge outfitted with an An-50 Ti rotor was employed for all sedimentation velocity (SV) experiments. The rotor housed conventional double-sector charcoal-filled epon centerpieces within the sample cells and contained either sapphire (Rayleigh interference optics) or quartz (absorption optics) windows. The absorption wavelength for optical detection was 280 nm and the interferometer laser wavelength was 660 nm. The samples were centrifuged at 42,000 rpm and 20 °C until sedimentation was complete. SEDNTERP[57] was employed to calculate the buffer viscosity ($\eta$), buffer density ($\rho$), and protein partial specific volume (v-bar) values at 20 °C based on a

database of known values available via the Internet (http://www.jphilo.mailway.com). The sedimentation coefficients were subsequently calculated by fitting the sedimentation velocity data using SEDFIT. The continuous distribution $c(s)$ Lamm equation model, which accounts for protein diffusion, was employed.[58] The sedimentation coefficients generated by this approach were confirmed by using DCDT+.[50,60] The apparent sedimentation coefficient distribution, $g(s^*)$, was generated from 22-26 scans with a peak broadening limit of 60 kDa using DCDT+.

All SV window assemblies were loaded with 410 μL of buffer reference and 400 μL of peptide sample, and the buffers and samples were prepared immediately before the SV runs. In one set of experiments, samples of $HD5_{ox}$, the $HD5[Ser^{3,31}]_{ox}$ and $HD5[Ser^{10,30}]_{ox}$ regioisomers, and $HD5[Ser^{hexa}]$ were prepared at pH 7 in 10 mM sodium phosphate buffer. A solution of 1N HCl was employed to adjust pH. Starting from a lyophilized peptide sample, a concentrated stock solution of each peptide was prepared from buffer that was filtered through a 0.45 μm membrane. In microcentrifuge tubes, aliquots of the peptide stock solution were diluted to 400 μL with buffer to provide the desired concentrations and subsequently transferred to the AUC sample cells. Samples at the following peptide concentrations were prepared and analyzed: $HD5_{ox}$, 30, 50, 80, 115, 120, 183, 186, 283, 301, 303, 424, and 437 μM; $HD5[Ser^{3,31}]_{ox}$ (5-20)(10-30), 60, 62, 65, 90, and 131 μM; $HD5[Ser^{3,31}]_{ox}$ (5-30)(10-20), 105, 136, and 201 μM; $HD5[Ser^{3,31}]_{ox}$ (5-10)(20-30), 74, 105, 153, and 210 μM; $HD5[Ser^{10,30}]_{ox}$ (3-20)(5-31), 153, 180, 224, and 236 μM; $HD5[Ser^{10,30}]_{ox}$ (3-31)(5-20), 57, 232, and 396 μM; $HD5[Ser^{hexa}]$, 90 and 91μM.

Additional SV experiments were conducted to evaluate the consequences of pH, salt, and buffer components on the sedimentation of $HD5_{ox}$. In all cases, the 400-μL solutions were prepared as described above and the buffer pH was adjusted by using 1 N HCl. To determine the effect of pH, samples of $HD5_{ox}$ in 10 mM sodium phosphate buffer were adjusted to pH values of 6 (161 μM), 4 (131 μM), and 2 (194 μM). To ascertain the effect of NaCl, samples of $HD5_{ox}$ at pH 7 in 10 mM sodium phosphate buffer containing 50 mM (183, 283 μM), 150 mM (181, 278 μM), and 500 mM (178, 270 μM) NaCl were prepared. To evaluate the effects of buffer choice and divalent cations, sedimentation of $HD5_{ox}$ was investigated at pH 7 in 20 mM Tris-HCl or 20 mM HEPES buffer with or without 50 mM $MgCl_2$ or $CaCl_2$. For the experiments in Tris buffer, the $HD5_{ox}$ concentrations were 126 and 210 μM (no divalent cations), 170 and 236 μM (+Mg), or 128 and 157 μM (+Ca). For the experiments in HEPES buffer, the $HD5_{ox}$ concentrations were 191 and 256 μM (no divalent cations), 131 and 190 μM (+Mg), and 191 and 212 μM (+Ca).

Hydrodynamic modeling computations were performed with HYDROPRO[61] to calculate sedimentation coefficients for the $HD5_{ox}$ monomer, dimer, and tetramer (Table S3). Both the $HD5_{ox}$ monomer NMR solution structure presented in this work and the reported $HD5_{ox}$ crystal structure (PDB: 1ZMP)[10] were employed in hydrodynamic modeling. All HYDROPRO calculations used the buffer density (ρ) and buffer viscosity (η) values for water at 20 °C, and a partial specific volume (v-bar) of 0.7087 mL/g for $HD5_{ox}$. Equation 1 was employed to calculate sedimentation coefficients for $HD5_{ox}$ modeled as a smooth, compact, and spherical peptide in water at 20 °C using the classical combination of the Svedberg and Stokes equation.[58] The values are reported in Tables S4. Equation 1 states

$$S_{sphere} = 0.012 \frac{M^{2/3}\left(1 - \bar{\nu}\,\rho\right)}{\eta^{-1/3}} \quad (1)$$

where $s_{sphere}$ is the sedimentation coefficient for an ideally sedimenting sphere in S units, M is in units of Daltons, $\bar{\nu}$ is in milliliters per gram, and ρ in grams per milliliter. To ascertain

the maximum shape asymmetry from a sphere, the minimum frictional ratios were calculated with Equation 2

$$S_{sphere}/S_{20,w} = f/f_0 \quad (2)$$

where $s_{20,w}$ is the sedimentation coefficient for the peptide in water at 20 °C, $f$ is the experimental frictional coefficient, and $f_0$ is the minimal frictional coefficient. The maximum shape asymmetry was determined for $HD5_{ox}$ in different buffers, HD5[$Ser^{hexa}$], HD5[$Ser^{3,31}$]$_{ox}$ and HD5[$Ser^{10,30}$]$_{ox}$. Each $f/f_0$ analysis for the disulfide deletion mutants was performed by using the average $s_{20,w}$ value determined from all regioisomeric disulfide pairings (Table S5).

### Sedimentation Equilibrium Experiments

The Beckman XL-I Analytical Ultracentrifuge outfitted with an An-50 Ti rotor described above was employed for all sedimentation equilibrium (SE) experiments. The absorption wavelength for optical detection was 280 nm and the instrument was maintained at 20 °C. Samples (400 μL) of $HD5_{ox}$ were prepared in 10 mM sodium phosphate buffer at pH 8 (183, 230, and 283 μM), 7 (165, 187, 225, 238, 283, and 288 μM), 6 (210 and 330 μM), 4 (236, and 288 μM), and 2 (189, 238, and 293 μM) as described above. Equilibrium profiles were established at rotor speeds of 20,000, 25,000, and 36,000 rpm based on sedimentation coefficients of ~1.8 S obtained from the SV experiments.[62] Upon equilibrium establishment, 10 scans with 5 replicates were recorded.

SEDNTERP[57] was employed to calculate the buffer viscosity (η), buffer density (ρ), and protein partial specific volume ($\bar{\nu}$) values at 20 °C as described above. Molecular weights were determined by global fitting of the multi-speed equilibrium data across at all loading concentrations at a given pH value using the program SEDPHAT.[63] The Species Analysis model and Single Species of an Interacting System model, both with mass conservation, were employed for data analysis with the bottom of the sample sector assigned as a floating parameter. To further verify whether each least squares curve-fitting procedure converged to a global minimum, the alternate methods of Simplex, Marquardt-Levenberg, and simulated annealing were employed to assess any change in the global reduced chi-squared value.

## RESULTS

### Peptide Stability in the Presence of *S. aureus*

Figure 2 presents the analytical HPLC traces obtained for supernatants of *S. aureus* cultures treated with $HD5_{ox}$, HD5[$Ser^{3,31}$] (5-10)(20-30), and HD5[$Ser^{hexa}$]. Traces for additional mutants are provided as Supporting Information (Figures S5-S6). In all cases, the peak corresponding to the peptide of interest exhibited comparable intensity whether or not *S. aureus* was included in the well. No new peaks in the analytical HPLC traces attributable to peptide degradation formed. These observations demonstrate that $HD5_{ox}$ and the disulfide mutant peptides are stable under the conditions previously employed for assaying antibacterial activity against *S. aureus*.[12] The attenuated activity of the mutant peptides reported previously results from neither peptide degradation nor disulfide bond reshuffling to an inactive form during the course of the assay.[12]

### Overexpression and Purification of Isotopically-labeled Peptides

$^{15}N$- and $^{13}C$,$^{15}N$-labeled $HD5_{ox}$ were obtained in yields of ca. 100 μg/L culture following overexpression of $His_6$ fusion proteins in M9 minimal media containing a vitamin supplement, Ni-NTA purification, $His_6$ tag cleavage, purification of the reduced form, and oxidative folding. This procedure was extended to the HD5[$Ser^{3,31}$] and HD5[$Ser^{10,30}$]

peptides, which were obtained in yields of ca. 100 and ca. 300 μg/L, respectively. All isotopically-labeled peptides were obtained in high purity (Figures S1-S4) and the identities were confirmed by mass spectrometry (Table S2). Although adequate for NMR studies, these yields are lower than the yields reported for peptide overexpression in nutrient-rich medium.[12] This decreased yield is largely attributed to variability in culture growth, ascertained by $OD_{600}$ values, in minimal media. In several instances, the $OD_{600}$ value remained ≤ 0.7 following induction and continued incubation at 37 °C. This phenomenon was unpredictable, and we therefore collected the cell pellets ca. 5.5 h after induction and independent of $OD_{600}$ value at that time point. The HD5[$Ser^{5,20}$] peptides were not considered in this work because only low yields of the unlabeled regioisomers were achieved previously in nutrient-rich medium.[12]

## NMR Solution Structure Determination of $HD5_{ox}$

A preliminary $^{1}H,^{15}N$-HSQC spectrum of $^{15}N$-$HD5_{ox}$ in 90:10 $H_2O/D_2O$ revealed thirty-one well-resolved amide resonances, which supported the presence of one folded species in solution (Figure 3). In contrast, markedly decreased peak dispersion was observed for $^{15}N$-$HD5_{red}$ in 90:10 $H_2O/D_2O$ containing 20 μM TFA (Figure 3), indicating that $HD5_{red}$ is unfolded. The loss of fold upon peptide reduction is in agreement with prior circular dichroism studies of HD5,[12] and a qualitative comparison of the $^{1}H,^{15}N$-HSQC spectra of oxidized and reduced human β-defensin 1.[64] Screenings of sample conditions and acquisition parameters to delineate the optimal conditions for data collection and solution structure determination were subsequently conducted. The $^{1}H,^{15}N$-HSQC spectra obtained for $^{15}N$-$HD5_{ox}$ prepared in Tris or sodium phosphate buffer over the pH range of 5 to 7 were markedly different than the spectra of the unbuffered sample presented in Figure 3. Specifically, peaks were broader, less dispersed, and more heterogeneous in intensity for the buffered samples (Figures S9,S10). Differences in the $^{1}H,^{15}N$-HSQC spectra were also observed for unbuffered $^{15}N$-$HD5_{ox}$ prepared in 90:10 $H_2O/D_2O$ that was pH adjusted with HCl or TFA (Figure S11-S13). Variations in acquisition temperature and sample concentration had negligible impact on chemical shift dispersion over the evaluated ranges (Figure S12). These exploratory studies highlighted the importance of sample preparation on dynamic exchange events, and further spectroscopic experiments were conducted in 90:10 $H_2O/D_2O$ with the sample pH adjusted to 4.0 by TFA addition.

2-D homonuclear NOESY and TOCSY spectra were employed for initial $^{15}N$-$HD5_{ox}$ sequence-specific assignments, using the established methods of Wüthrich.[65] These spectra where insufficient to complete sequence-specific assignment because of significant attenuation of many backbone amide signals and poor NOE data, which were most likely the results of exchange broadening. Only ca. 50% of the molecule could be assigned by using this approach, and with low confidence. A sample of $^{13}C,^{15}N$-$HD5_{ox}$ was therefore prepared, and standard triple-resonance spectra (HNCO, HNCA, HNCACO) were collected to aid in backbone assignment. In addition, 3-D $^{13}C$-edited and 3-D $^{15}N$-edited NOESY spectra of $^{13}C,^{15}N$-$HD5_{ox}$ were recorded. These spectra, together with the homonuclear experiments, permitted almost complete sequence-specific assignment of the $HD5_{ox}$ backbone (87.5% of the backbone assigned) and an overall assignment of 89.7% for the entire molecule (Figure S14). This assignment was sufficient for structure determination. Further assignment was hampered by exchange broadening of signals (Figure S15, *vide infra*). Additionally, backbone chemical shift assignment of the heavy nuclei provided information on backbone dihedral angles. Preliminary CYANA structure calculations confirmed beta-sheet elements, and the H-bonding network was established by the proximity of interresidue NOEs. Previous crystallographic studies of synthetic $HD5_{ox}$ revealed the α-disulfide bonding pattern of$Cys^{3}$—$Cys^{31}$, $Cys^{5}$—$Cys^{20}$, and $Cys^{10}$—$Cys^{30}$.[10] In this work, characteristic inter-cysteine NOEs were observed between these pairs of cysteine residues

(Table S6, Figure S16). Moreover, initial structure calculations were consistent with this arrangement of the disulfide bonds without explicitly declaring them in the calculation. Covalent disulfide bonding restraints for $Cys^3$—$Cys^{31}$, $Cys^5$—$Cys^{20}$, and $Cys^{10}$—$Cys^{30}$ were therefore included in the final structure calculations (Figure S17). The final collection of 20 lowest energy structures was generated with explicit water refinement, which provided a backbone RMSD of 0.135 Å for the heavy atom backbone over the full length of the peptide (Table 1). The solution structure was determined for the $HD5_{ox}$ monomer because intermolecular NOEs were not reliably observed. The lack of intermolecular NOEs most likely results from exchange broadening of the Hα signals at the dimer interface (*vide infra*).

The overall fold of $HD5_{ox}$ exhibits a three-stranded beta-sheet characteristic of α-defensins (Figure 4). Strand β1 consists of residues 4-6, β2 is comprised of residues 15-22, and β3 extends from residues 25-31. Strands β2 and β3 are connected by a tight beta type-I turn defined by $Ser^{23}$-$Gly^{24}$ (Figures 1 and 4). The three beta-sheets constitute 65% of the tertiary structure (Figure S18). This beta-sheet content is greater than that observed for Crp4 (34%)[43] and similar to the beta-sheet content (60%) of HNP3.[66] Residues 7-14 form a loop of irregularly-structured secondary structure. The presence of the $Arg^6$—$Glu^{14}$ salt bridge is apparent from observed NOE interactions with neighboring residues. The five additional Arg residues are positioned on one face of the structure, and on the opposite side of the predominantly hydrophobic $Ser^{15}$-$Ile^{22}$ beta sheet (Figures 4C and S19). This clustering of hydrophobic and hydrophilic residues provides amphipathic character.

## NMR Solution Studies of $HD5_{ox}$ Quaternary Structure and Dynamics

Evaluation of the oligomerization state of the $^{13}C,^{15}N$-$HD5_{ox}$ NMR sample was evaluated through $T_1/T_2$ data, a $^{15}N$-TRACT experiment, and calculations of rotational correlation time ($T_c$). $T_1$ values were measured using the standard inversion-recovery method, and $T_2$ data were obtained from a Carr-Purcell-Meiboom-Gill (CPMG) relaxation dispersion experiment. $T_1/T_2$ data for the well-structured beta-turn region were used to estimate correlation times. The average $T_2$ value from this beta-turn region defined by $Ile^{22}$-$Leu^{26}$ is 181.2 ms, which corresponds to a $T_c$ of ca. 3.5 – 3.7 ns. The $T_c$ was also determined using the [$^{15}N$,$^1H$]-TRACT method, which relies on the transverse relaxation optimized spectroscopy (TROSY) principle.[67] This method gives estimates of $T_c$ that are independent of exchange phenomenon, which can complicate the interpretation of $T_2$ measurements. This approach afforded a $T_c$ value of ca. 4.1 ns, which is in good agreement with the $T_2$ analysis of the beta-turn loop and estimates a molecular weight of ca. 6.8 kDa. Both methods indicate that $HD5_{ox}$ exists as a dimer under the NMR sample conditions.

Outside of the $Ile^{22}$-$Leu^{26}$ beta-turn region, the $T_2$ values are highly variable whereas the $T_1$ values are nearly equal (Figure 5A). Many residues exhibit $T_2$ values that are shorter than the T values for the $Ile^{22}$-$Leu^{26}$ 2 beta-turn region (e.g. residues 5-7, 10-14, 16-17, 19, 27, 30, 31), indicating that these residues may undergo conformational exchange broadening (Figure 5B). To determine whether these residues are indeed exchange broadened, we plotted $T_2$ values versus $T_1$ values (Figure 5C). In addition, we overlaid the theoretical values of $T_2$ and $T_1$ for a range of correlation times using the standard 'Model Free' formalism of Lipari and Szabo[68,69] and for various order parameters ($S^2$ values) for data collection at 600 MHz. A $S^2$ value of 1.0 indicates a rigid structure whereas lower $S^2$ values point to flexibility on the microsecond or faster timescale. Figure 5C reveals that many residues fall to the left of the $S^2$=1.0 line, indicating that these residues are most likely exchange broadened on a time scale of milliseconds. This large amount of exchange broadening is consistent with the difficulties encountered in assigning the backbone of $HD5_{ox}$.

### NMR Solution Studies of Disulfide Deletion Mutants

1-D $^{1}$H and 2-D $^{1}$H,$^{15}$N-HSQC NMR spectra were recorded for all regioisomers of HD5[Ser$^{3,31}$]$_{ox}$ and HD5[Ser$^{10,30}$]$_{ox}$ (Figures S7,S8,S20-S26). In all cases, the chemical shift dispersion of the amide HN region was less than 1 ppm and comparable to the dispersion observed for unstructured HD5$_{red}$ (Figure 3). Moreover, many of these spectra exhibited greater than thirty-one amide resonances, which suggested that multiple species exist in aqueous solution at pH 4. The disulfide deletion mutant peptides each lack structural organization in aqueous solution. As a result, no further NMR spectroscopic characterization of these peptides was pursued.

### Sedimentation Velocity Studies of HD5$_{ox}$ Quaternary Structure

A series of SV experiments were conducted to evaluate the sedimentation of behavior of HD5$_{ox}$ under a variety of conditions, and the results from all SV experiments are summarized as Supporting Information (Tables S7-S11 and Figures S27-S30). At pH 7 in 10 mM sodium phosphate buffer, conditions similar to those routinely employed for *in vitro* defensin antibacterial activity assays,[12] a single peak at 1.8 S is observed over the range $s$20,w = 0.7 – 3.7 S in both the Gaussian fit of the observed $g$(s*) peak and in $c(s)$ (Figure 6). The Gaussian fit supports the existence of a single species, and the single peak in $c(s)$ precludes the presence of fast association kinetics between various oligomeric states.[32] To evaluate whether the S-value exhibits concentration dependence, HD5$_{ox}$ samples ranging from 30 to 437 μM were evaluated (Figures S27). In all cases, one sedimentation coefficient of ca. 1.8 S was obtained by the $g(s^*)$, $c(s)$, and dc/dt methods (Table S7), which supports a monodisperse oligomerization state at pH 7 over this concentration range, and also suggests a dissociation constant below 30 μM for the 1.8 S species.

The HD5$_{ox}$ S-value decreased as the pH was lowered from 7 to 2 across a range of sample concentrations (10 mM sodium phosphate buffer). Sedimentation coefficients of 1.8 S (pH 7.0), 1.6 S (pH 6.0), 1.2 S (pH 4.0), and 1.0 S (pH 2.0) were obtained by DCDT+ analysis, which provided evenly-distributed single-Gaussian fitting of the absorbance raw data of as corrected $s_{20,w}$ values (Table S8, Figures S28).

Substitution of phosphate buffer with Tris or HEPES buffer had negligible effect on the sedimentation of HD5$_{ox}$ at pH 7 (Tables S9,S10 and Figure S29). Average sedimentation coefficients of ca. 1.6 S over a range of peptide concentrations were obtained for HD5$_{ox}$ in Tris or HEPES buffer, respectively. Moreover, millimolar concentrations of Mg(II) and Ca(II) had negligible impact on the HD5$_{ox}$ sedimentation coefficient when added to either Tris or HEPES buffer at pH 7.0 (Tables S9,S10 and Figure S29). These data demonstrate that physiological concentrations of Mg(II) and Ca(II) do not influence HD5$_{ox}$ quaternary structure in aqueous solution. Moreover, up to 500 mM NaCl had no effect on the sedimentation coefficient of HD5$_{ox}$ at pH 7 (10 mM sodium phosphate buffer) (Table S10, Figure S30).

Using both the NMR solution structure and the x-ray crystal structure of HD5$_{ox}$ as models, sedimentation coefficients were estimated using HYDROPRO to be 0.66 S (monomer), 1.16 S (dimer), and 1.71 S (tetramer) (Table S3). The HD5$_{ox}$ homodimer observed in the crystalline form was employed to calculate the dimer sedimentation coefficient. Two different models of HD5$_{ox}$ tetramers were generated from the crystallographic structure and evaluated, and each provided the same predicted S-value. A comparison of the experimentally-obtained and calculated S-values indicates that HD5$_{ox}$ exists in a tetrameric form in aqueous buffer at neutral pH at concentrations ≥30 μM. Moreover, this comparison suggests that pH modulates HD5$_{ox}$ quaternary structure, and suggest that dimers predominate at lower pH.

Equation 2 was employed to determine minimum frictional ratios ($f/f_o$) and thereby provide a semi-quantitative analysis of maximum shape asymmetry for $HD5_{ox}$. In all cases the $f/f_0$ ratio was ~1.2, which suggests that the HD5 oligomers exhibit globular shape. No extended elongation is predicted for the tetrameric form.

### Sedimentation Equilibrium Studies of $HD5_{ox}$ Quaternary Structure

SE experiments were subsequently conducted to determine the molecular weight of the $HD5_{ox}$ species observed to sediment at 1.8 S (Figures 7 and S31-S36). Samples of varying $HD5_{ox}$ concentrations were used to collect absorbance equilibrium profiles at speeds appropriate for a ~14 kDa globular peptide (10 mM sodium phosphate buffer, pH 7.0). After global analysis of six different $HD5_{ox}$ samples at pH 7, each at three different rotor speeds, the calculated molecular weight was determined to be 14,363 Da. This value is within 1% error of the theoretical molecular weight of a $HD5_{ox}$ tetramer (14,328 Da). The globally-fit value has a standard deviation of ±32 Da and at the 95% confidence interval ranged from 14,472 – 14,716 Da using a Monte-Carlo analysis of fit (Table S12). This analysis was extended to $HD5_{ox}$ samples at varying pH, and the molecular weight calculations of samples prepared at pH 4.0, 6.0, and 8.0 also converged to tetrameric molecular weights; however, the global reduced chi-squared values increased with decreasing pH from 7.0 to 4.0. The data obtained at pH 4.0 could be fit using the molecular weight of a $HD5_{ox}$ dimer, but the residuals of the fit were poor compared to those obtained after converging to a tetramer molecular weight (Figures S34,S35). Moreover, a markedly different sedimentation profile of $HD5_{ox}$ at pH 2.0 was observed and afforded a best-fit molecular weight of 7,079 Da (Figure 7). This molecular weight corresponds to a dimer within 2% error (7,164 Da). These results confirm that the $HD5_{ox}$ oligomerization state in aqueous solution is pH-dependent with dimers predominating at relatively low pH and tetramers forming at higher pH values.

### Sedimentation Velocity Studies of Disulfide Mutant Quaternary Structure

To evaluate the consequence of disulfide bond deletion on quaternary structure, SV experiments were performed with the regioisomers of $HD5[Ser^{3,31}]_{ox}$ and $HD5[Ser^{10,30}]_{ox}$, in addition to $HD5[Ser^{hexa}]$, at pH 7.0 (10 mM sodium phosphate buffer). Regardless of peptide concentration and method of analysis (e.g. *c(s)* and dc/dt), each peptide exhibited sedimentation coefficient values that were markedly and consistently lower than those of wild-type $HD5_{ox}$ obtained under the same conditions (Table S5 and Figures S37-S39). The sedimentation coefficient values for the $HD5[Ser^{3,31}]_{ox}$ and $HD5[Ser^{10,30}]_{ox}$ regioisomers averaged ca. 0.80 S and ca. 0.90 S, respectively. These values fall between the HYDROPRO-calculated S-values for the HD5 dimer (1.16 S) and monomer (0.71 S) The hexa mutant sedimentation coefficient averaged ca. 0.67. These results demonstrate that loss of the $Cys^3$—$Cys^{31}$ or $Cys^{10}$—$Cys^{30}$ disulfide bond, or linearization of the peptide backbone, prohibits tetramer formation at pH 7.0. Linearization affords a monomeric, random coli species. Loss of one disulfide bond results in one or more unfolded species that may be described as lower-order oligomers. HYDROPRO calculations of energy-minimized random coil structures of these disulfide deletion mutants were in agreement with the presence of monomeric species.

## DISCUSSION

In this work, we present the results of biophysical investigations designed to probe the solution structure and oligomeric properties of the human host-defense peptide $HD5_{ox}$ and a family of disulfide deletion mutants. First, multidimensional NMR spectroscopy afforded the $HD5_{ox}$ solution structure (Figure 3), and confirmed a dimeric oligomerization state under the NMR sample conditions. Second, analytical ultracentrifugation experiments conducted over a range of pH values and in the presence and absence of millimolar Na(I),

Ca(II), and Mg(II) delineated factors that contribute to $HD5_{ox}$ oligomerization in aqueous solution. One particularly noteworthy observation is the effects of buffer and pH on the formation and disassembly of $HD5_{ox}$ tetramers (Figure 7). Lastly, complementary studies of disulfide array mutant peptides and $HD5_{red}$ confirmed that the native α-defensin scaffold, defined by the tridisulfide array, is essential for structural rigidity and the formation of well-defined oligomeric species. Taken together, these studies afford insights into the solution behavior, oligomerization properties, and disulfide array of $HD5_{ox}$, which provides a basis for further understanding its biological activities and evaluating its structure and function in the context of other α-defensin family members.

All α-defensins share the same regiospecific pairing of cysteine residues (I-VI, II-IV, III-V, with Cys numbered sequentially from N- to C-terminus) and a three-stranded β-sheet fold. Other conserved features include an invariant Gly residue ($Gly^{18}$ in HD5) and the Arg—Glu salt bridge. Nevertheless, the primary amino acid sequences and overall charges of α-defensins are variable, which afford diverse structural dynamics and biological activities, and necessitates evaluation of α-defensin family members on a case-by-case basis.

Atomic-level solution structural characterization is important for elucidating structure/function relationships of antimicrobial peptides.[70] Comparison of the $HD5_{ox}$ solution structure with other α-defensin structures reveals noteworthy similarities and differences. Crystallographic characterization of $HD5_{ox}$ provided several different monomeric forms (PDB: 1ZMP).[10] Overlay of the $HD5_{ox}$ solution structure and the $HD5_{ox}$ crystallographic monomers shows marked topological agreement and provides a RMSD of 1.042 Å for heavy backbone atoms (Figure S40). Likewise, the backbones of $HD5_{ox}$ and HNP3 (PDB: 1DFN) are highly similar with a RMSD of 1.073 Å (Figure S41). The cysteine residues of HNP3 and HD5 share primary amino acid sequence positions, and both peptides exhibit well-defined N- and C-termini in solution (Figure S41). Although $HD5_{ox}$ shares the overall α-defensin fold of rabbit kidney-defensin RK-1[71] and murine cryptdin-4,[43] the latter two peptides exhibit markedly increased conformational flexibility at the N- and C-termini that results from the positioning of the I and VI cysteine residues (Figure S41B). The biological ramifications of variable termini flexibility in α-defensins are currently unclear; studies of β-defensins indicated that termini flexibility may contribute to oligomerization.[72]

The disulfide array imposes the α-defensin topology exhibited by HD5 and other family members, and also confers protease resistance. The NMR studies of the disulfide deletion mutants are in agreement with prior NMR characterization of cryptdin-4 disulfide array mutants[42] and reduced HBD-1,[64] and further confirm that disulfide deletion results in a loss of peptide fold. Moreover, the $^{1}H,^{15}N$-HSQC spectra of mutants lacking a single disulfide bond indicate that multiple species are present in solution. Guided by the sedimentation coefficients obtained for the $HD5[Ser^{3,31}]_{ox}$ and $HD5[Ser^{10,30}]_{ox}$, which fall between the calculated S-values of the $HD5_{ox}$ monomer and dimer, we contend that the speciation may result from mixtures of oligomeric species.

Recent mutagenesis studies have highlighted the importance of both electrostatics and hydrophobicity in human α-defensin antibacterial action.[4,35-37] Electrostatic and hydrophobicity depictions of select α-defensins are provided as Supporting Information (Figures S42-S47). The primary amino acid sequence of HD5 contains six arginine residues (Figure 1). $Arg^{6}$ is involved in the salt-bridge, and the five remaining Arg residues are distributed along one side of the tertiary surface (Figure 4C). The opposite face contains a largely hydrophobic and slightly concave area. This region houses $Val^{19}$, $Ile^{22}$, and $Leu^{29}$ in addition to $Cys^{3}$—$Cys^{31}$ and $Cys^{5}$—$Cys^{20}$. Only one charged residue, $Glu^{21}$, is located on this face (Figure S43), and it is adjacent to the tight beta type-I turn. $HD5_{ox}$ therefore exhibits amphipathic character. Many defensins are amphipathic in nature, and this attribute

is generally accepted to be important for membrane interactions and antimicrobial activity.[4] Nevertheless, the number and arrangement of Arg residues in α-defensins are variable, and $HD5_{ox}$ exhibits a relatively well-defined cluster of Arg residues on one topological surface as compared to HNPs and cryptdin-4 (Figure S19,S44). This feature is likely relevant to the $HD5_{ox}$ mechanisms of antimicrobial action. Along such lines, replacement of select Arg residues with Ala or Lys attenuated the antibacterial activity of $HD5_{ox}$ against several bacterial species.[27]

The propensity of defensins to self-associate and form oligomers is considered to be important for various biological functions, including bacterial membrane disruption and antiviral activity.[4] Nevertheless, few thorough investigations of defensin quaternary structure are in the literature, and how sample conditions contribute to the observed oligomerization states are largely unknown. Biophysical characterization of the θ-defensin retrocyclin-2 exemplified the importance of buffer composition for oligomerization.[73] The first crystallographic characterization of an α-defensin revealed HNP3 in a dimeric form,[66] and this structural feature was hypothesized to be important for bacterial membrane permeabilization. Later solid-state NMR spectroscopic studies of HNP1 suggested a dimer pore mechanism of membrane disruption.[74] Recent investigations demonstrated the importance of HNP1 dimerization in antibacterial activity, anthrax lethal factor inhibition, and binding to HIV-1 gp120.[37] A model of HNP1 tetramerization was also proposed in this work. Crystallographic characterization of other human α-defensins, including HD5 and HNP4, also revealed dimeric forms.[10] Dimers of human β-defensin HBD-3[72] and the plant defensin NaD1[75] have been observed in solution. In contrast, monomers of cryptdin-4,[76] RK-1[71] and human β – defensins[72] HBD-1 and -2 were identified. Self-assembly of HD6 "nanonets," or higher-order oligomers, was recently described and implicated in protection of the intestinal mucosa from bacterial invasion.[77] Taken together, these studies indicate that defensin oligomerization is highly variable and likely dependent on the sample conditions, making direct comparisons difficult and complicating predictions of oligomeric state.

The dimeric oligomerization state of $HD5_{ox}$ in the NMR sample (90:10 $H_2O/D_2O$, pH 4) was first indicated by analysis of $T_2$ values and later confirmed by a [$^{15}N$,$^{1}H$]-TRACT experiment. Indeed, self-association of $HD5_{ox}$ was observed by crystallography and surface plasmon resonance (SPR).[10,35,78] A dissociation constant of ca. 2 μM was obtained from SPR experiments conducted at pH 7.4 and in the presence of 150 mM NaCl, attributed to dimer formation; evidence for higher-order oligomers was reported at $HD5_{ox}$ concentrations greater than ca. 8 μM.[78] Recent mutagenesis studies indicated a hydrophobic mode of dimerization.[35] The structural studies presented in this work further confirm the importance of hydrophobicity in $HD5_{ox}$ quaternary structure. The $^{13}C$-edited NOESY spectrum revealed a number of exchange-broadened Hα signals, including those corresponding to residues $Cys^{20}$-$Glu^{21}$ housed on the outermost sheet of the β-bulge. Exchange broadening of Hα signals was also observed for residues 7 and 10 of the loop. Exchange broadening was judged to occur at these positions because a lack of recordable data corresponding to these atoms was obtained in the $^{13}C$ edited NOESY spectrum. Lastly, the backbone $^{15}N$ $T_2$ measurements indicate that specific regions of the peptide undergo conformer exchange broadening (Figure 5B). Asymmetric tumbling is an alternative explanation for the differential levels of $T_2$ relaxation because this phenomenon results in longer $T_2$ times away from the center of mass. $HD5_{ox}$ is not a spherical molecule, however we contend that a spherical model for tumbling is indeed appropriate and differential tumbling along unequal axes does not account for the distribution of $T_2$ times measured (Figure S48). Residues 22-24 comprise the beta turn, are the most distant from the center of mass. These residues exhibit some of the most ideal $T_2$ values (e.g. close to the $S^2$=1.0 line, Figure 5C). The order parameter plots exhibited in Figure 5C are based on the Lipari and Szabo 'model free' theory,[68,69] which assumes spherical tumbling, and suggest that a spherical model for

$HD5_{ox}$ tumbling is appropriate for the beta turn residues. In contrast, short $T_2$ values are observed for many residues in loop 7-14; however, this loop also traces along points that are distant from the center of mass; these $T_2$ values are inconsistent asymmetric tumbling. We therefore conclude that $T_2$ times in $HD5_{ox}$ are indicative of a dimeric interface that is exchanging between free and bound forms on the millisecond time scale.

In contrast, the analytical ultracentrifugation studies presented in this work indicate that $HD5_{ox}$ exists as a tetramer at >30 μM in buffered aqueous solution at neutral pH (Figures 6 and 7). Taking the sedimentation equilibrium results into account, we speculate that the significant peak broadening and heterogeneous signal intensities observed in the $^{1}H,^{15}N$-HSQC NMR spectra of $^{15}N$-$HD5_{ox}$ prepared in buffered solutions resulted from tetramer formation. Further sedimentation velocity experiments indicated that the tetramer was unaffected by varying the sample concentration or buffer composition (phosphate vs. Tris vs. HEPES), or by addition of millimolar concentrations of the divalent cations Na(I), Ca(II) and Mg(II). We chose to investigate the consequences of cation addition because the antibacterial activity of HD5 is "salt-sensitive." Like many defensins, addition of millimolar concentrations of NaCl to assay buffer results in attenuated antibacterial activity *in vitro*.[22] This phenomenon is typically attributed to a salt-induced disruption of electrostatic interactions between the defensin and negatively-charged bacterial cell surface. The results presented in this work demonstrate that up to 500 mM NaCl does not perturb $HD5_{ox}$ quaternary structure over the peptide concentration range tested, suggesting that disrupted oligomerization does not contribute to attenuated antibacterial activity in the presence of salt. In contrast, the absence or presence of buffer and also pH modulate the $HD5_{ox}$ oligomerization state. In phosphate buffer, $HD5_{ox}$ oligomerization is influenced by pH. The pH effect is evidenced by the S-values obtained from the SV measurements and in the SE data (Figure 7). The conclusion that $HD5_{ox}$ is best described as a dimer at pH 4 in unbuffered solution and as a tetramer in the presence of 10 mM sodium phosphate at pH 5 illustrates the importance of solution composition when evaluating defensin oligomerization states. Indeed, prior solution studies of retrocyclin-2 revealed buffer-dependence.[73] A trimer was obsereved at pH 7.4 in either phosphate or Tris buffer whereas, in unbuffered solution, the trimer was only observed at higher peptide concentrations. Further investigations are required to elucidate the molecular basis for this pH-dependent self-association from dimer to tetramer in addition to residues that comprise the tetramer interface of $HD5_{ox}$.

HD5 is released from Paneth cells into the human small intestinal lumen where it contributes to mucosal immunity. Concentrations of HD5 at the point of secretion in the small intestine are estimated to be ca. 280 μM (10 mg/mL).[79] The NMR and AUC studies presented in this work span this concentration range. Moreover, the AUC investigations cover a pH range relevant to the small intestine in physiological and pathological states. This environment is relatively neutral to slightly alkaline environment under healthy conditions largely as a result of bicarbonate production by the pancreas and mucosa, and becomes more acidic during inflammation.[80] Although the compositions of aqueous buffer and the intestinal mucosa/lumen differ substantially, and various small molecules such as fatty acids present in the gut may influence oligomerization, the results from this investigation suggest that HD5 may exist as a tetramer in the healthy gut. Moreover, it is intriguing to speculate that alterations in HD5 oligomerization, and hence function, may occur as a result of pH fluctuations in the gut, e.g. during intestinal inflammation as a result of a more acidic environment.

We previously reported that deletion of a single disulfide bond in $HD5_{ox}$ results in loss of antibacterial activity against *S. aureus*.[12] Taking the current peptide stability and biophysical investigations into account, we conclude that this attenuated activity results from disrupted peptide fold and quaternary structure. Identifying particular cellular targets of $HD5_{ox}$ for a

variety of bacterial species and characterizing the $HD5_{ox}$/target interaction(s) are required to further elucidate precisely how $HD5_{ox}$ contributes to innate immunity and human health.

## Supplementary Material

Refer to Web version on PubMed Central for supplementary material.

## Acknowledgments

This work was supported by NIH Grant DP2OD007045 (EMN) from the Office of the Director, National Institutes of Health and NIH Grant P01 GM047467 (GW) from the National Institute of General Medical Sciences. The FBML is supported by NIH Grant EB-002026 from the National Institute of Bio-Medical Imaging and Bioengineering of the NIH. The content is solely the responsibility of the authors and does not necessarily represent the official views of the National Institutes of Health. Support was also received from the Department of Chemistry at MIT (EMN). NMR instrumentation housed in the MIT-DCIF is maintained by funding from the National Science Foundation (CHE-9808061). The MIT Biophysical Instrumentation Facility for the Study of Complex Macromolecular Systems is supported by Grants NSF-0070319 and NIH GM68762.

## Acknowledgments

We thank Ms. Debby Pheasant for assistance with the AUC experimental setup, Dr. Robert Radford and Dr. Nozomi Ando for helpful discussions about AUC, and Dr. Tsyr-Yan (Dharma) Yu for assistance in the collection and analysis of the TRACT NMR data.

## ABBREVIATIONS

| | |
|---|---|
| **AUC** | Analytical ultracentrifugation |
| **CFU** | Colony forming unit |
| **HD5** | Human α-defensin 5 |
| **$HD5_{red}$** | Reduced human defensin 5 |
| **$HD5_{ox}$** | Oxidized human defensin 5 |
| **HNP** | Human neutrophil peptide (an α-defensin) |
| **HSQC** | Heteronuclear single quantum coherence |
| **IPTG** | Isopropyl-β-D-thiogalactopyranoside |
| **LB** | Luria Broth |
| **NOESY** | Nuclear Overhauser effect spectroscopy |
| **OD** | Optical density |
| **SE** | Sedimentation equilibrium |
| **SV** | Sedimentation velocity |
| **TFA** | Trifluoroacetic acid |
| **TOCSY** | Total correlation spectroscopy |
| **TROSY** | Transverse relaxation optimized spectroscopy |
| **TSB** | Trypticase soy broth |

## REFERENCES

1. Choi K-Y, Chow LNY, Mookherjee N. Cationic host defence peptides: Multifaceted role in immune modulation and inflammation. J. Innate Immun. 2012; 4:361–370. [PubMed: 22739631]

2. Hazlett L, Wu M. Defensins in innate immunity. Cell Tissue Res. 2011; 343:175–188. [PubMed: 20730446]
3. Niyonsaba F, Nagaoka I, Ogawa H. Human defensins and cathelicidins in the skin: Beyond direct antimicrobial properties. Crit. Rev. Immunol. 2006; 26:545–575. [PubMed: 17341194]
4. Lehrer RI, Lu W. alpha-Defensins in human innate immunity. Immunol. Rev. 2012; 245:84–112. [PubMed: 22168415]
5. Klotman ME, Chang TL. Defensins in innate antiviral immunity. Nat. Rev. Immunol. 2006; 6:447–456. [PubMed: 16724099]
6. Ganz T. Defensins: Antimicrobial peptides of innate immunity. Nat. Rev. Microbiol. 2003; 3:710–720.
7. Schneider JJ, Unholzer A, Schaller M, Schäfer-Korting M, Korting HC. Human defensins. J. Mol. Med. 2005; 83:587–595. [PubMed: 15821901]
8. Pazgier M, Li X, Lu W, Lubkowski J. Human defensins: Synthesis and structural properties. Curr. Pharm. Des. 2007; 13:3096–3118. [PubMed: 17979752]
9. Cunliffe RN. alpha-Defensins in the gastrointestinal tract. Mol. Immunol. 2003; 40:463–467. [PubMed: 14568393]
10. Szyk A, Wu Z, Tucker K, Yang D, Lu W, Lubkowski J. Crystal structures of human alpha-defensins HNP4, HD5, and HD6. Protein Sci. 2006; 15:2749–2760. [PubMed: 17088326]
11. Rajabi M, de Leeuw E, Pazgier M, Li J, Lubkowski J, Lu W. The conserved salt bridge in human alpha-defensin 5 is required for its precursor processing and proteolytic stability. J. Biol. Chem. 2008; 283:21509–21518. [PubMed: 18499668]
12. Wanniarachchi YA, Kaczmarek P, Wan A, Nolan EM. Human defensin 5 disulfide array mutants: Disulfide bond deletion attenuates antibacterial activity against Staphylococcus aureus. Biochemistry. 2011; 50:8005–8017. [PubMed: 21861459]
13. Jones DE, Bevins CL. Paneth cells of the human small intestine express an antimicrobial peptide gene. J. Biol. Chem. 1992; 267:23216–23225. [PubMed: 1429669]
14. Mallow EB, Harris A, Salzman N, Russell JP, DeBerardinis RJ, Ruchelli E, Bevins CL. Human enteric defensins: Gene structure and developmental expression. J. Biol. Chem. 1996; 271:4038–4045. [PubMed: 8626737]
15. Porter EM, Liu L, Oren A, Anton PA, Ganz T. Localization of human intestinal defensin 5 in Paneth cell granules. Infect. Immun. 1997; 65:2389–2395. [PubMed: 9169779]
16. Wehkamp J, Chu H, Shen B, Feathers RW, Kays RJ, Lee SK, Bevins CL. Paneth cell antimicrobial peptides: Topographical distribution and quantification in human gastrointestinal tissues. FEBS Lett. 2006; 580:5344–5350. [PubMed: 16989824]
17. Quayle AJ, Porter EM, Nussbaum AA, Wang YM, Brabec C, Yip K-P, Mok SC. Gene expression, immunolocalization, and secretion of human defensin-5 in human female reproductive tract. Am. J. Pathol. 1998; 152:1247–1258. [PubMed: 9588893]
18. Spencer JD, Hains DS, Porter E, Bevins CL, DiRosario J, Becknell B, Wang H, Schwaderer AL. Human alpha defensin 5 expression in the human kidney and urinary tract. PLoS One. 2012; 7:e31712. [PubMed: 22359618]
19. Porter EM, Bevins CL, Ghosh D, Ganz T. The multifaceted Paneth cell. Cell. Mol. Life Sci. 2002; 59:156–170. [PubMed: 11846026]
20. Cunliffe RN, Rose FRAJ, Keyte J, Abberley L, Chan WC, Mahida YR. Human defensin 5 is stored in precursor form in normal Paneth cells and is expressed by some villous epithelial cells and by metaplastic Paneth cells in the colon in inflammatory bowel disease. Gut. 2001; 48:176–185. [PubMed: 11156637]
21. Ghosh D, Porter E, Shen B, Lee SK, Wilk D, Drazba J, Yadav SP, Crabb JW, Ganz T, Bevins CL. Paneth cell trypsin is the processing enzyme for human defensin-5. Nat. Immunol. 2002; 3:583–590. [PubMed: 12021776]
22. Porter EM, van Dam E, Valore EV, Ganz T. Broad-spectrum antimicrobial activity of human intestinal defensin 5. Infect. Immun. 1997; 65:2396–2401. [PubMed: 9169780]
23. Ericksen B, Wu Z, Lu W, Lehrer RI. Antibacterial activity and specificity of the six human alpha-defensins. Antimicrob. Agents Chemother. 2005; 49:269–275. [PubMed: 15616305]

24. Salzman NH, Ghosh D, Huttner KM, Paterson Y, Bevins CL. Protection against enteric salmonellosis in transgenic mice expressing a human intestinal defensin. Nature. 2003; 422:522–526. [PubMed: 12660734]
25. Salzman NH, Hung K, Haribhai D, Chu H, Karlsson-Sjöberg J, Amir E, Teggatz P, Barman M, Hayward M, Eastwood D, Stoel M, Zhou Y, Sodergren E, Weinstock GM, Bevins CL, Williams CB, Bos NA. Enteric defensins are essential regulators of intestinal microbial ecology. Nat. Immunol. 2010; 11:76–83. [PubMed: 19855381]
26. Wehkamp J, Salzman NH, Porter E, Nuding S, Weichenthal M, Petras RE, Shen B, Schaeffeler E, Schwab M, Linzmeier R, Feathers RW, Chu H, Lima H, Fellermann K, Ganz T, Stange EF, Bevins CL. Reduced Paneth cell alpha-defensins in ileal Crohn's disease. Proc. Natl. Acad. Sci. U. S. A. 2005; 102:18129–18134. [PubMed: 16330776]
27. de Leeuw E, Rajabi M, Zou GZ, Pazgier M, Lu W. Selective arginines are important for the antibacterial activity and host cell interaction of human alpha-defensin 5. FEBS Lett. 2009; 583:2507–2512. [PubMed: 19589339]
28. Seo, E.-j.; Weibel, S.; Wehkamp, J.; Oelschlaeger, TA. Construction of recombinant E. coli Nissle 1917 (EcN) strains for the expression and secretion of defensins. Int. J. Med. Microbiol. 2012; 302:276–287. [PubMed: 22748509]
29. Shi J. Defensins and Paneth cells in inflammatory bowel disease. Inflamm. Bowel Dis. 2007; 13:1284–1292. [PubMed: 17567878]
30. Buck CB, Day PM, Thompson CD, Lubkowski J, Lu W, Lowy DR, Schiller JT. Human alpha-defensins block papillomavirus infection. Proc. Natl. Acad. Sci. U. S. A. 2006; 103:1516–1521. [PubMed: 16432216]
31. Smith JG, Nemerow GR. Mechanism of adenovirus neutralization by human alpha-defensins. Cell Host Microbe. 2008; 3:11–19. [PubMed: 18191790]
32. Gounder AP, Wiens ME, Wilson SS, Lu W, Smith JG. Critical determinants of human alpha-defensin 5 activity against non-enveloped viruses. J. Biol. Chem. 2012; 287:24554–24562. [PubMed: 22637473]
33. de Leeuw E, Burks SR, Li X, Kao JPY, Lu W. Structure-dependent functional properties of human defensin 5. FEBS Lett. 2007; 581:515–520. [PubMed: 17250830]
34. Wei G, de Leeuw E, Pazgier M, Yuan W, Zou G, Wang J, Ericksen B, Lu W-Y, Lehrer RI, Lu W. Through the looking glass, mechanistic insights from enantiomeric human defensins. J. Biol. Chem. 2009; 284:29180–29192. [PubMed: 19640840]
35. Rajabi M, Ericksen B, Wu XJ, de Leeuw E, Zhao L, Pazgier M, Lu W. Functional determinants of human enteric alpha-fefensin HD5: Crucial role for hydrophobicity at dimer interface. J. Biol. Chem. 2012; 287:21615–21627. [PubMed: 22573326]
36. Wei G, Pazgier M, de Leeuw E, Rajabi M, Li J, Zou G, Jung G, Yuan W, Lu W-Y, Lehrer RI, Lu W. Trp-26 imparts functional versatility to human alpha-defensin HNP1. J. Biol. Chem. 2010; 285:16275–16285. [PubMed: 20220136]
37. Pazgier M, Wei G, Ericksen B, Jung G, Wu Z, de Leeuw E, Yuan W, Szmacinski H, Lu W-Y, Lubkowski J, Lehrer RI, Lu W. Sometimes It takes two to tango: Contributions of dimerization to functions of human alpha-defensin HNP1 peptide. J. Biol. Chem. 2012; 287:8944–8953. [PubMed: 22270360]
38. Zhao L, Ericksen B, Wu X, Zhan C, Yuan W, Li X, Pazgier M, Lu W. Invariant Gly residue is important for alpha-defensin folding, dimerization, and function: A case study of the human neutrophil alpha-defensin HNP1. J. Biol. Chem. 2012; 287:18900–18912. [PubMed: 22496447]
39. Mandal M, Nagaraj R. Antibacterial activities and conformations of synthetic alpha-defensin HNP-1 and analogs with one, two and three disulfide bridges. J. Pept. Res. 2002; 59:95–104. [PubMed: 11985703]
40. Zou GZ, de Leeuw E, Li C, Pazgier M, Li C, Zeng P, Lu W-Y, Lubkowski J, Lu W. Toward understanding the cationicity of defensins: Arg and Lys versus their noncoded analogs. J. Biol. Chem. 2007; 282:19653–19665. [PubMed: 17452329]
41. Tanabe H, Qu X, Weeks CS, Cummings JE, Kolusheva S, Walsh KB, Jelinek R, Vanderlick TK, Selsted ME, Ouellette AJ. Structure-activity determinants in Paneth cell alpha-defensins: Loss-of-

function in mouse cryptdin-4 by charge-reversal at arginine residue positions. J. Biol. Chem. 2004; 279:11976–11983. [PubMed: 14702345]

42. Maemoto A, Qu X, Rosengren KJ, Tanabe H, Henschen-Edman A, Craik DJ, Ouellette AJ. Functional analysis of the alpha-defensin disulfide array in mouse cryptdin-4. J. Biol. Chem. 2004; 279:44188–44196. [PubMed: 15297466]
43. Rosengren KJ, Daly NL, Fornander LM, Jönsson LMH, Shirafuji Y, Qu XQ, Vogel HJ, Ouellette AJ, Craik DJ. Structural and functional characterization of the conserved salt bridge in mammalian Paneth cell alpha-defensins: Solution structures of mouse cryptdin-4 and (E15D)-cryptdin-4. J. Biol. Chem. 2006; 281:28068–28078. [PubMed: 16857681]
44. Hadjicharalambous C, Sheynis T, Jelinek R, Shanahan MT, Ouellette AJ, Gizeli E. Mechanisms of alpha-defensin bactericidal action: Comparative membrane disruption by Cryptdin-4 and Its disulfide-null analogue. Biochemistry. 2008; 47:12626–12634. [PubMed: 18973303]
45. Andersson HS, Figueredo SM, Haugaard-Kedström LM, Bengtsson E, Daly NL, Qu X, Craik DJ, Ouellette AJ, Rosengren KJ. The alpha-defensin salt bridge induces backbone stability to facilitate folding and confer proteolytic resistance. Amino Acids. 2012 ahead of print.
46. Masuda K, Sakai N, Nakamura K, Yoshioka S, Ayabe T. Bactericidal activity of mouse alpha-defensin cryptdin-4 predominantly affects noncommensal bacteria. J. Innate Immun. 2011; 3:315–326. [PubMed: 21099205]
47. Studier FW. Protein production by auto-induction in high-density shaking cultures. Protein Expres. Purif. 2005; 41:207–234.
48. Hyberts SG, Takeuchi K, Wagner G. Poisson-gap sampling and forward maximum entropy reconstruction for enhancing the resolution and sensitivity of protein NMR data. J. Am. Chem. Soc. 2010; 132:2145–2147. [PubMed: 20121194]
49. Hyberts SG, Milbradt AG, Wagner AB, Arthanari H, Wagner G. Application of iterative soft thresholding for fast reconstruction of NMR data non-uniformly sampled with multidimensional Poisson Gap scheduling. J. Biomol. NMR. 2012; 52:315–327. [PubMed: 22331404]
50. Delaglio F, Grzesiek S, Vuister GW, Zhu G, Pfeifer J, Bax A. NMRpipe: A multidimensional spectral processing system based on Unix pipes. J. Biomol. NMR. 1995; 6:277–293. [PubMed: 8520220]
51. Goddard, TD.; Kneller, DG. SPARKY 3. University of California; San Francisco:
52. Keller, RLJ. Thesis. ETH Zürich no. 15947. Swiss Federal Institute of Technology Zürich; Zürich, Switzerland: 2005. Optimizing the process of NMR spectrum analysis and computer aided resonance assignment.
53. Cornilescu G, Delaglio F, Bax A. Protein backbone angle restraints from searching a database for chemical shift and sequence homology. J. Biomol. NMR. 1999; 13:289–302. [PubMed: 10212987]
54. Laskowski RA, MacArthur MW, Moss DS, Thornton JM. PROCHECK: a program to check the stereochemical quality of protein structures. J. App. Cryst. 1993; 26:283–291.
55. Pettersen EF, Goddard TD, Huang CC, Couch GS, Greenblatt DM, Meng EC, Ferrin TE. UCSF chimera - A visualization system for exploratory research and analysis. J. Comput. Chem. 2004; 25:1605–1612. [PubMed: 15264254]
56. Koradi R, Billeter M, Wüthrich K. MOLMOL: A program for display and analysis of macromolecular structures. J. Mol. Graphics. 1996; 14:51–55.
57. Laue M, Shah BD, Ridgeway TM, Pelletier SL. Analytical Ultracentrifugation in Biochemistry and Polymer Science, Royal Society of Chemistry, Edited by S. Harding and A. Rowe. 1992:90–125.
58. Lebowitz J, Lewis MS, Schuck P. Modern analytical ultracentrifugation in protein science: A tutorial review. Protein Sci. 2002; 11:2067–2079. [PubMed: 12192063]
59. Philo JS. A method for directly fitting the time derivative of sedimentation velocity data and an alternative algorithm for calculating sedimentation coefficient distribution functions. Anal. Biochem. 2000; 279:151–163. [PubMed: 10706784]
60. Schuck P. On the analysis of protein self-association by sedimentation velocity analytical ultracentrifugation. Anal. Biochem. 2003; 320:104–124. [PubMed: 12895474]
61. Ortega A, Amorós D, de la Torre JG. Prediction of hydrodynamic and other solution properties of rigid proteins from atomic- and residue-level models. Biophys. J. 2011; 101:892–898. [PubMed: 21843480]

62. Schuck, P.; Braswell, EH. Measurement of protein interactions by equilibrium ultracentrifugation. In: Coligan, JE.; Kruisbeek, A.; Margulies, DH.; Shevach, EM.; Strober, W., editors. Current Protocols in Immunology. Wiley; New York: 2000. p. 18.18.11-18.18.22.
63. Vistica J, Dam J, Balbo A, Yikilmaz E, Mariuzza RA, Rouault TA, Schuck P. Sedimentation equilibrium analysis of protein interactions with global implicit mass conservation constraints and systematic noise decomposition. Anal. Biochem. 2004; 326:234–256. [PubMed: 15003564]
64. Schroeder BO, Wu Z, Nuding S, Groscurth S, Marcinowski M, Beisner J, Buchner J, Schaller M, Stange EF, Wehkamp J. Reduction of disulphide bonds unmasks potent antimicrobial activity of human beta-defensin 1. Nature. 2011; 469:419–423. [PubMed: 21248850]
65. Wüthrich, K. NMR of Proteins and Nucleic Acids. Wiley; New York: 1986.
66. Hill CP, Yee J, Selsted ME, Eisenberg D. Crystal structure of defensin HNP-3, an amphiphilic dimer: Mechanisms of membrane permeabilization. Science. 1991; 251:1481–1485. [PubMed: 2006422]
67. Lee D, Hilty C, Wider G, Wüthrich K. Effective rotational correlation times of proteins from NMR relaxation interference. J. Mag. Res. 2006; 178:72–76.
68. Lipari G, Szabo A. Model-free approach to the interpretation of nuclear magnetic-resonance relaxation in macromolecules. 1. Theory and range of validity. J. Am. Chem. Soc. 1982; 104:4546–4559.
69. Lipari G, Szabo A. Model-free approach to the interpretation of nuclear magnetic-resonance relaxation in macromolecules. 2. Analysis of experimental results. J. Am. Chem. Soc. 1982; 104:4559–4570.
70. Bhattacharjya S, Ramamoorthy A. Multifunctional host defense peptides: functional and mechanistic insights from NMR structures of potent antimicrobial peptides. FEBS J. 2009; 276:6465–6473. [PubMed: 19817858]
71. McManus AM, Dawson NF, Wade JD, Carrington LE, Winzor DJ, Craik DJ. Three-dimensional structure of RK-1: A novel alpha-defensin peptide. Biochemistry. 2000; 39:15757–15764. [PubMed: 11123900]
72. Schibli DJ, Hunter HN, Aseyev V, Starner TD, Wiencek JM, McCray PB Jr. Tack BF, Vogel HJ. The solution structures of the human beta-defensins lead to a better understanding of the potent bactericidal activity of HBD3 against Staphylococcus aureus. J. Biol. Chem. 2002; 277:8279–8289. [PubMed: 11741980]
73. Daly NL, Chen Y-K, Rosengren KJ, Marx UC, Phillips ML, Waring AJ, Wang W, Lehrer RI, Craik DJ. Retrocyclin-2: Structural analysis of a potent anti-HIV theta-defensin. Biochemistry. 2007; 46:9920–9928. [PubMed: 17685559]
74. Zhang Y, Lu W, Hong M. The membrane-bound structure and topology of a human alpha-defensin indicate a dimer pore mechanism for membrane disruption. Biochemistry. 2010; 49:9770–9782. [PubMed: 20961099]
75. Lay FT, Mills GD, Poon IKH, Cowieson NP, Kirby N, Baxter AA, van der Weerden NL, Dogovski C, Perugini MA, Anderson MA, Kvansakul M, Hulett MD. Dimerization of plant defensin NaD1 enhances its antifungal activity. J. Biol. Chem. 2012; 287:19961–19972. [PubMed: 22511788]
76. Jing W, Hunter HN, Tanabe H, Ouellette AJ, Vogel HJ. Solution structure of cryptdin-4, a mouse Paneth cell alpha-defensin. Biochemistry. 2004; 43:15759–15766. [PubMed: 15595831]
77. Chu H, Pazgier M, Jung G, Nuccio S-P, Castillo PA, de Jong MF, Winter MG, Winter SE, Wehkamp J, Shen B, Salzman NH, Underwood MA, Tsolis RM, Young GM, Lu W, Lehrer RI, Bäumler AJ, Bevins CL. Human alpha-defensin 6 promotes mucosal innate immunity through self-assembled peptide nanonets. Science. 2012; 337:477–481. [PubMed: 22722251]
78. Lehrer RI, Jung G, Ruchala P, Andre S, Gabius HJ, Lu W. Multivalent binding of carbohydrates by the human alpha-defensin, HD5. J. Immunol. 2009; 183:480–490. [PubMed: 19542459]
79. Ayabe T, Satchell DP, Wilson CL, Parks WC, Selsted ME, Ouellette AJ. Secretion of microbicidal alpha-defensins by intestinal Paneth cells in response to bacteria. Nat. Immunol. 2000; 1:113–118. [PubMed: 11248802]

80. Nugent SG, Kumar D, Rampton DS, Evans DF. Intestinal luminal pH in inflammatory bowel disease: possible determinants and implications for therapy with aminosalicylates and other drugs. Gut. 2001; 48:571–577. [PubMed: 11247905]

81. Grishaev A, Bax A. An empirical backbone-backbone hydrogen-bonding potential in proteins and its applications to NMR structure refinement and validation. J. Am. Chem. Soc. 2004; 126:7281–7292. [PubMed: 15186165]

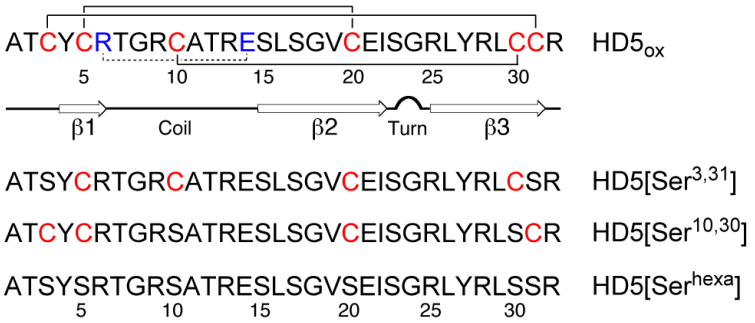


**Figure 1.**

Primary amino acid sequences of $HD5_{ox}$ and the mutant peptides employed in this work. The numbers refer to amino acid position. The Cys residues comprising the $Cys^{3}$—$Cys^{31}$, $Cys^{5}$—$Cys^{20}$, and $Cys^{10}$—$Cys^{30}$ disulfide linkages (solid lines) are shown in red and the residues of the $Arg^{6}$—$Glu^{14}$ salt-bridge (dashed line) are indicated in blue. The secondary structure depiction is based on the NMR solution structure presented in this work. Throughout the main text, the regiospecific disulfide linkages that define each mutant peptide are indicated in parantheses.

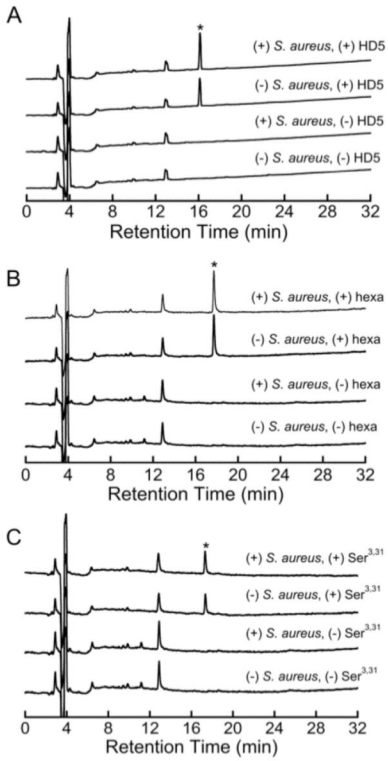


**Figure 2.**

Analytical HPLC traces of *S. aureus* culture supernatants (10 mM sodium phosphate buffer supplemented with 1% TSB, pH 7.4) treated with 20 μM of $HD5_{ox}$ or a mutant peptide for 1 h at 37 °C. (A) $HD5_{ox}$. (B) $HD5[Ser^{hexa}]$. (C) $HD5[Ser^{3,31}]$ (5-10)(20-30). Absorption at 220 nm was monitored with a reference wavelength of 500 (A) or 360 nm (B and C) (10-60% B in 30 min). In each panel, the star indicates the peak corresponding to the defensin peptide. Traces for the remaining HD5 mutants are provided as Supporting Information.

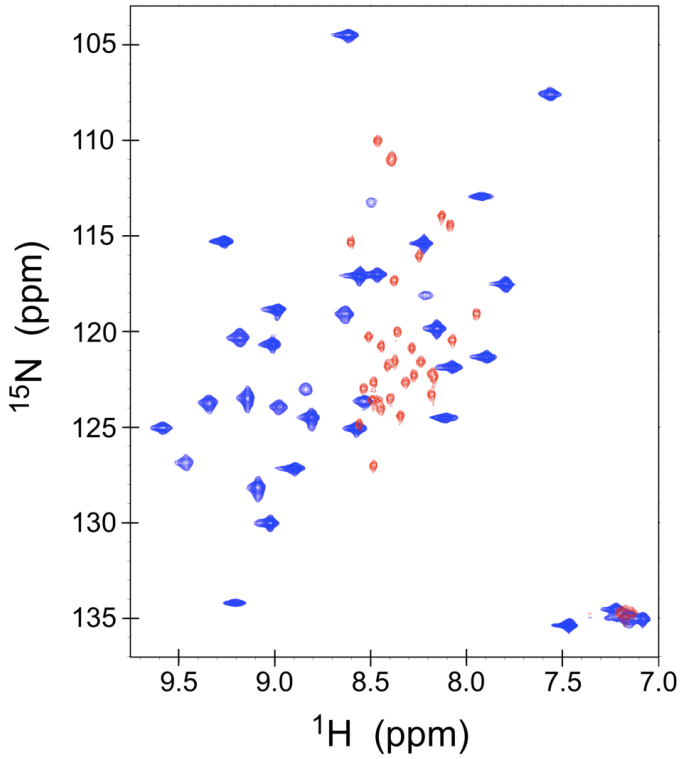


**Figure 3.**
Overlay of $^{15}$N-HD5$_{ox}$ (blue) and $^{15}$N-HD5$_{red}$ (red) $^{1}$H,$^{15}$N-HSQC spectra recorded on a 600 MHz spectrometer. The concentration of HD5$_{red}$ was 650 μM the sample was prepared in 90:10 $H_2O/D_2O$ containing 20 μM TFA. The HD5$_{ox}$ sample concentration was 460 μM and the sample was prepared in 90:10 $H_2O/D_2O$ immediately after HPLC purification and lyophilization, and no pH adjustment was performed.

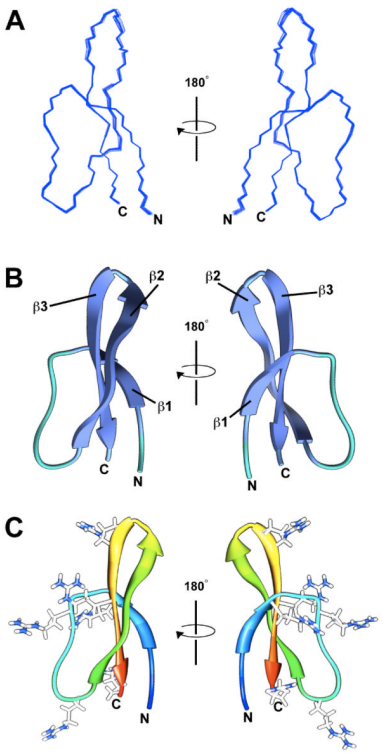


**Figure 4.**

NMR solution structure of 340 μM $^{13}C,^{15}N$-$HD5_{ox}$ in 90:10 $H_2O/D_2O$ at pH 4. (A) Overlay of the best twenty structures selected from 400 calculated conformers. RMSD for backbone atoms, 0.135 Å; RMSD for heavy atoms, 1.352 Å. (B) Ribbon diagrams illustrating the β-sheet structure of $HD5_{ox}$. (C) Depiction of the arrangement of the six Arg residues.

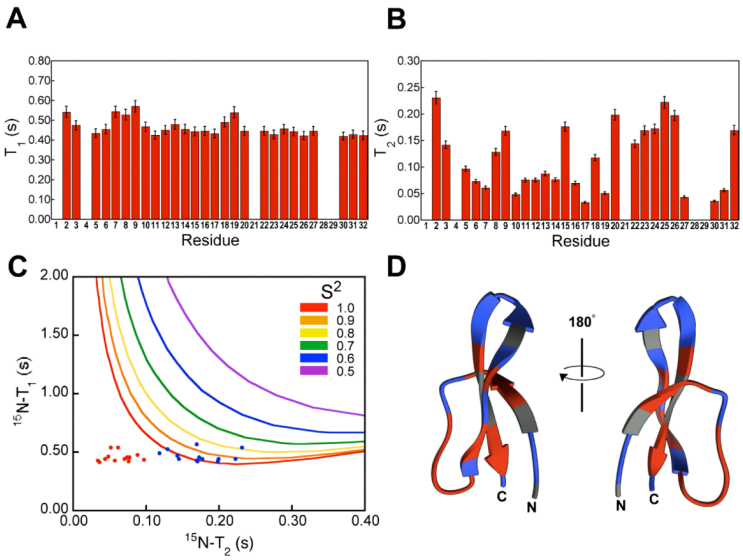


**Figure 5.**

Relaxation studies and dynamics of 340 μM $^{13}$C,$^{15}$N-HD5$_{ox}$ in 90:10 $H_2O/D_2O$ at pH 4. (A) $T_1$ data. (B) $T_2$ data. (C) Plot of $T_2$ versus $T_1$ with theoretical order parameters ($S^2$ values) for data collected at 600 MHz. Red dots: Residues with unusually short $T_2$ values ($T_2$ < 0.12 s). Blue dots: Residues with $T_2$ > 0.12 s. (D) NMR structure of HD5$_{ox}$ where $T_2$ values < 0.12 s or > 0.12 s are colored in red or blue, respectively. The grey regions indicate unobserved residues.

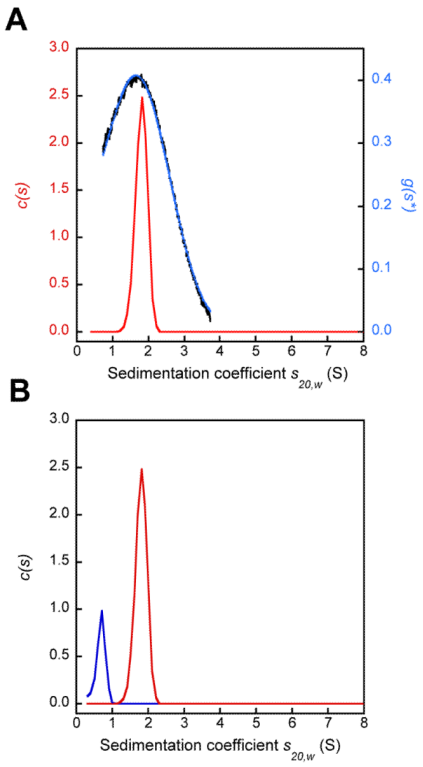


**Figure 6.**

Sedimentation coefficient determination for $HD5_{ox}$ and HD5[$Ser^{hexa}$] at pH 7 (10 mM sodium phosphate buffer) by analytical ultracentrifugation. (A) Sedimentation coefficient determination for 301 μM $HD5_{ox}$. The black curve is the apparent sedimentation coefficient distribution g(s*). The blue curve is the single Gaussian fit of this data. The red curve is the diffusion-deconvoluted sedimentation coefficient distribution $c(s)$. These analyses provide a S-value of 1.8 S and indicate that $HD5_{ox}$ is tetrameric under these experimental conditions. (B) Comparison of the diffusion-deconvoluted sedimentation coefficient distributions of 91 μM HD5[$Ser^{hexa}$] (blue) and 301 μM $HD5_{ox}$ (red). Additional sedimentation velocity data for $HD5_{ox}$ and mutant peptides are provided as Supporting Information.

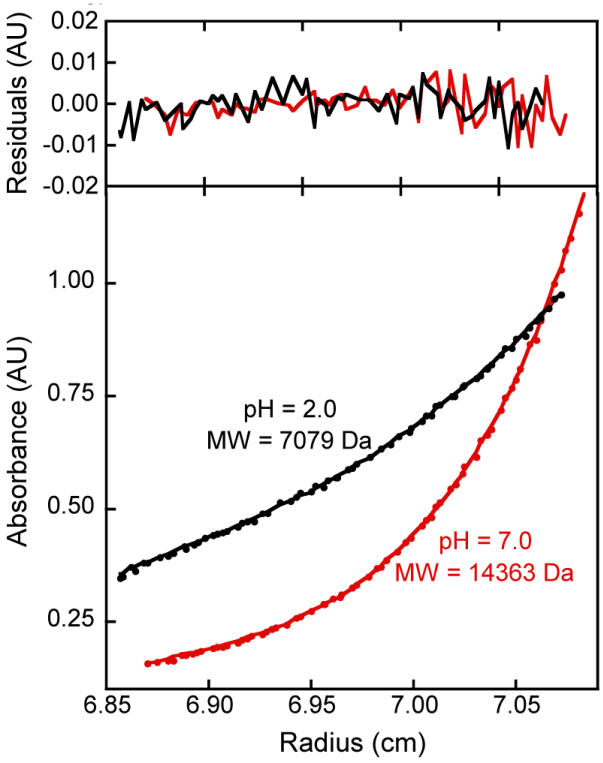


**Figure 7.**

Sedimentation equilibrium of 189 μM $HD5_{ox}$ at pH 2 (black) and 187 μM $HD5_{ox}$ at pH 7 (red) in 10 mM sodium phosphate buffer. Top panel: The residuals of the fits. Bottom panel: Sedimentation equilibrium data (circles) and fits (lines) at a rotor speed of 36,000 rpm. Additional sedimentation equilibrium data for $HD5_{ox}$ and mutant peptides are provided as Supporting Information.

**Table 1**

Structure Statistics for the Solution Structure of $HD5_{ox}$

| | <SA> | $(\overline{SA})_r$ |
|---|---|---|
| R.m.s. deviations from NOE restraints (Å) [a] | | |
| all (421) | 0.032±0.003 | 0.056 |
| sequential [ \| i - j \| = 1] (151) | 0.035±0.004 | 0.052 |
| medium range [ \| i - j \| ≤ 4] (53) | 0.027±0.005 | 0.074 |
| long range [ \| i - j \| ≥ 5 ] (133) | 0.024±0.006 | 0.066 |
| intra-residue (84) | 0.035±0.008 | 0.045 |
| R.m.s. deviations from dihedral angles restraints (°) [b] | 0.044 ± 0.017 | 0.877 |
| Deviation from idealized covalent geometry | | |
| bonds (Å) | 0.011 ± 0.006 | 0.004 |
| angles (°) | 0.573 ± 0.081 | 0.523 |
| impropers (°) | 0.250 ± 0.073 | 0.493 |
| Ramachandran results (%) [c] | | |
| most favorable region | 85.6 ± 3.8 | 92.6 |
| additionally allowed region | 14.4 ± 3.8 | 7.4 |
| generously allowed region | 0.0 ± 0.0 | 0.0 |
| disallowed region | 0.0 ± 0.0 | 0.0 |
| Coordinate Precision (Å) [d,e] | | |
| Protein backbone | 0.135 ± 0.034 | |
| Protein heavy atoms | 0.806 ± 0.102 | |

[a] None of the structures exhibited distance violations greater than 0.5 Å or dihedral angle violations greater than 5°.

[b] The experimental dihedral angle restraints were as follows: 26 $\varphi$, 25 $\psi$ and 15 $\chi 1$ angular restraints.

[c] Determined using the program PROCHECK.[38]

[d] The coordinate precision is defined as the average atomic root mean square deviation (RMSD) of the 20 individual SA structures and their mean coordinates. Backbone atoms are N, Cα, and C'.

[e] Structure calculations also included 15 hydrogen bonds. These bonds where included in X-PLOR structure calculations as HBDB terms as described in ref. 81.